A Deep Learning Network to Retrieve Ocean Hydrographic Profiles from Combined Satellite and In Situ Measurements

B. Buongiorno Nardelli[1]

[1]Istituto di Scienze Marine, Consiglio Nazionale delle Ricerche.

Corresponding author: Bruno Buongiorno Nardelli (bruno.buongiornonardelli@cnr.it)

Key Points:

- A novel deep learning technique to retrieve the 3D ocean hydrography combining satellite and in situ observations is presented
- A stacked Long Short-Term Memory network is coupled to a Monte Carlo dropout method to estimate vertical profiles and associated errors
- Applying the technique to 2010-2018 data collected in the North Atlantic leads to a significant improvement in the reconstruction accuracy

Abstract

An efficient combination of the data collected by multiple instruments and platforms is needed to obtain accurate 3D ocean state estimates, representing a fundamental step to describe ocean dynamics and its role in the Earth climate system and marine ecosystems. Observations can either be assimilated in ocean general circulation models or used to feed data-driven reconstructions and diagnostic models. Here we describe an innovative deep learning algorithm that projects sea surface satellite data at depth after training with sparse co-located in situ vertical profiles. The technique is based on a stacked Long Short-Term Memory neural network, coupled to a Monte-Carlo dropout approach, and is applied here to the measurements collected between 2010 and 2018 over the North Atlantic Ocean. The model provides hydrographic vertical profiles and associated uncertainties from corresponding remotely sensed surface estimates, outperforming similar reconstructions from simpler statistical algorithms and feed-forward networks.

Plain Language Summary

Being able to monitor the ocean's interior structure is crucial to assess the impact of ocean dynamics on the Earth climate and marine ecosystems. Available observations, acquired either from satellite sensors looking at the sea surface or from sparse in situ measurements of the water column, can only provide partial views of the 3D ocean state if analysed separately, due to their instrumental and sampling limitations. Taking advantage of recent advances in artificial neural network implementations, we present here a deep learning algorithm that is able to efficiently exploit sensors' synergy and retrieve the vertical hydrographic structure of the sea from remotely sensed data, including an estimate of associated uncertainties.

1 Introduction

Ocean dynamics comprises several processes (inter)acting over a wide range of spatial and temporal scales, which may influence the Earth climate and contribute to modulate marine ecosystem functioning. Notably, several crucial processes contributing to the transport of momentum, energy, chemicals and marine organisms cannot be fully understood unless repeated views of the 3D ocean state and surface forcings are available. This is particularly relevant for processes in the mesoscale to sub-mesoscale range, given their intrinsic 3D nature (McWilliams, 2019; Pilo et al., 2018; Stukel et al., 2017). In turn, the dynamical response and feedbacks of these processes to natural and anthropogenic pressures also remains largely uncertain. However, given both theoretical and practical limitations of available technologies, observations can only provide partial views of the ocean state, especially if analysed separately. Monitoring 3D ocean processes from observation-based reconstructions thus requires ingenious combinations of data acquired from different sensors looking at the sea surface from space, and from sparse in situ measurements collected throughout the water column.

Scientists have followed two main complementary approaches to provide a description of 3D ocean dynamics: the assimilation of observations in numerical models and the combination of purely data-driven reconstructions and diagnostic models. Both strategies are affected by strengths and weaknesses, though.

The data assimilation in prognostic models can guarantee the ocean state to evolve in a consistent way with the physics represented by the model (Carrassi et al., 2018; Moore et al., 2019; Stammer et al., 2016). Models, however, are affected by uncertainties in initialization and forcings, and need parameterizations of sub-grid scale processes, which may lead to inaccurate representations of the physics, especially when aiming to reconstruct long timeseries for decadal/climatological studies (due to grid size limitations and subsequent need to parameterize also mesoscale processes, e.g. Forget et al., 2015). In general, models' ability to reproduce non-assimilated observations is further hindered by the difficulty to properly account for model and observation representativeness and errors.

Data-driven approaches are based on a synergic use of different satellite, in-situ measurements and diagnostic models. They can reduce the differences between reconstructed and independent observations (for 2D examples see Ciani et al., 2020; Rio et al., 2016; Ubelmann et al., 2016), but usually allow only a much simpler description of the dynamics with respect to general circulation models (sometimes limited to zero or first order balances, as geostrophy and quasi-geostrophy, or simple Ekman models). Data-driven 3D reconstruction techniques that found a systematic application are based on purely empirical and/or statistical regressions/analyses (Buongiorno Nardelli et al., 2012, 2017, 2018; Guinehut et al., 2004, 2012; Hutchinson et al., 2016; Meijers et al., 2011; Meinen and Watts, 2000), eventually coupled to dynamical diagnostic tools (for full 3D examples see Mulet et al., 2012; Buongiorno Nardelli, 2020). Methodologies derived within the surface quasi-geostrophy framework make much stronger assumptions on the ocean vertical stratification, though providing interesting theoretical perspectives (Fresnay et al., 2018; Isern-Fontanet and Hascoët, 2014; LaCasce and Wang, 2015; Lapeyre, 2017; Liu et al., 2019; Wang et al., 2013). More recently, mixed approaches have also been explored (Yan et al., 2020).

All data driven approaches share the objective to project surface information at depth, starting from synoptic satellite observations and some prior knowledge of the hydrography. Despite the recent advancements in machine learning algorithms implementation and a growing interest in the possibilities opened by artificial intelligence for data science, only few attempts have been carried out until now to address this specific objective with artificial neural networks (e.g. Bao et al., 2019; Gueye et al., 2014; Lu et al., 2019; Sammartino et al., 2018; Wu et al., 2012), either based on generalized regression neural networks, self-organizing maps or feed-forward neural networks. Models based on neural networks have also been proposed to "augment" observed vertical profiles with variables that have not been directly measured (e.g. Ballabrera-Poy et al., 2009; Bittig et al., 2018; Sauzède et al., 2016, 2017).

In this paper, a stacked Long Short-Term Memory (LSTM, Hochreiter and Schmidhuber, 1997) network is coupled to a Monte Carlo dropout approach and used to project surface data at depth after training with sparse co-located in situ vertical profiles. LSTM is a deep learning algorithm particularly suited to exploit sequential information as those present in hydrographic profiles. Dropout provides both a regularization strategy, when applied during training, and a "Bayesian" inference approximation if applied during both training and testing (Gal and Ghahramani, 2016). As such, the technique proposed here is able to provide both vertical hydrographic profiles and uncertainties on the predicted values.

This work was carried out within the European Space Agency World Ocean Circulation project (ESA-WOC), as a preparatory step for the development of a daily 3D reconstruction of the dynamics in the North Atlantic (down to 1500 m depth) at 1/10° spatial resolution, covering the period between 2010 and 2018. As such, the network was trained and tested taking as target (output) the measurements collected by Argo profilers and CTD casts within a wide portion of the North Atlantic over that period. Co-located satellite-derived sea surface temperature, sea surface salinity and absolute dynamic topography values (extracted from operational and experimental products) were used as input data.

The performance of the proposed LSTM network has been assessed by keeping part of the in situ profiles as independent reference observations during test. Root mean squared errors have been estimated from LSTM profiles, from climatological data and multivariate Empirical Orthogonal Function reconstructions (mEOF-r, as in Buongiorno Nardelli et al., 2017), as well as from the output of simpler feed-forward networks.

2 Data

2.1 Surface data

The SST used in the present study is the level 4 (L4, i.e. interpolated) multi-year reprocessed Operational Sea Surface Temperature and Sea Ice Analysis (OSTIA) developed by U.K. Met Office and distributed (upon free registration) through the Copernicus Marine Environment Monitoring Service (CMEMS, http://marine.copernicus.eu/services-portfolio/access-to-products/, product_id=SST_GLO_SST_L4_REP_OBSERVATIONS_010_011). OSTIA combines the reprocessed ESA SST CCI, C3S, EUMETSAT, REMSS and OSPO satellite data, and in-situ data from HadIOD and provides daily maps of foundation SST (i.e. not affected by the diurnal cycle). The analysis runs an optimal interpolation (OI) algorithm on a 1/20° regular grid (Roberts-Jones et al., 2012). OSTIA was sub-sampled here to 1/10° resolution, and resulting grid was used also for the pre-processing of the other surface datasets (see the SST example in figure 1a).

The SSS data have been developed within ESA-WOC project (https://doi.org/10.5281/zenodo.3943813). They have been obtained by adapting to the 1/10° North Atlantic grid the multidimensional optimal interpolation algorithm used to retrieve CMEMS global dataset (http://marine.copernicus.eu/services-portfolio/access-to-products/, product_id: MULTIOBS_GLO_PHY_REP_015_002, dataset_id: dataset-sss-ssd-rep-weekly). This algorithm interpolates SMOS observations and in situ SSS observations considering a space-time-thermal decorrelation function, estimated by including information from high-pass filtered daily SST data (Droghei et al., 2016; Buongiorno Nardelli, 2012). This multivariate approach effectively increases the SSS resolution by using satellite SST differences to constrain the surface patterns (see figure 1b). Here, we ingested the SMOS L3OS 2Q debiased daily salinity disseminated by the Centre Aval de Traitement des Données SMOS (CATDS, 2017), OSTIA SST data and CORA5.2 surface values (see section 2.2) as input data, and used CMEMS weekly SSS dataset to build our background field (linearly interpolating it in time between the two closest analysis dates, and upsizing to the 1/10° grid through a cubic spline). All other interpolation parameters are set as in Droghei et al. (2018).

The Absolute Dynamic Topography (ADT) data considered here are based on the altimeter Sea Level Anomaly (SLA) product provided by SSALTO/Data Unification and Altimeter Combination System (DUACS). They are obtained by adding a Mean Dynamic

Topography (Rio et al., 2014) to the SLA field, and are distributed by CMEMS as reprocessed data (http://marine.copernicus.eu/services-portfolio/access-to-products/, product_id: SEALEVEL_GLO_PHY_L4_REP_OBSERVATIONS_008_047). ADT has been upsized here to the ESA-WOC 1/10°x1/10° grid through a cubic spline (see example in figure 1c). ADT data have been pre-processed to make them consistent with insitu steric heights. The adjustment is carried out as in Buongiorno Nardelli et al. (2017), namely by regressing steric heights and co-located ADT data in the neighbourhood of each grid point, considering matchups within a temporal window of $\pm$10 days.

2.2 Vertical profiles

The vertical hydrographic profiles have been taken from the quality controlled Argo and CTD profiles produced by CMEMS CORA 5.2 (http://marine.copernicus.eu/services-portfolio/access-to-products/, product_id: INSITU_GLO_TS_REP_OBSERVATIONS_013_001_b, doi: 10.17882/46219TS1, Szekely et al., 2019). The data considered here are restricted to the 2010-2018 period, and were interpolated through a spline on a regularly spaced vertical grid (with 10 m intervals). Steric heights have been computed taking 1500 m as reference level.

2.3 Climatology

Temperature and salinity monthly climatological fields computed by the World Ocean Atlas 2013 have been used to convert all daily observations to anomaly fields (see section 3). These climatologies are estimated on a 1/4° x 1/4° grid by applying an objective analysis algorithm (Locarnini et al., 2013; Zweng et al., 2013). The values in the first 1500 m, provided on 125 levels, have been interpolated through a spline on a regularly spaced vertical grid (with 10 m intervals), and upsized to the 1/10° ESA-WOC grid through a cubic spline.

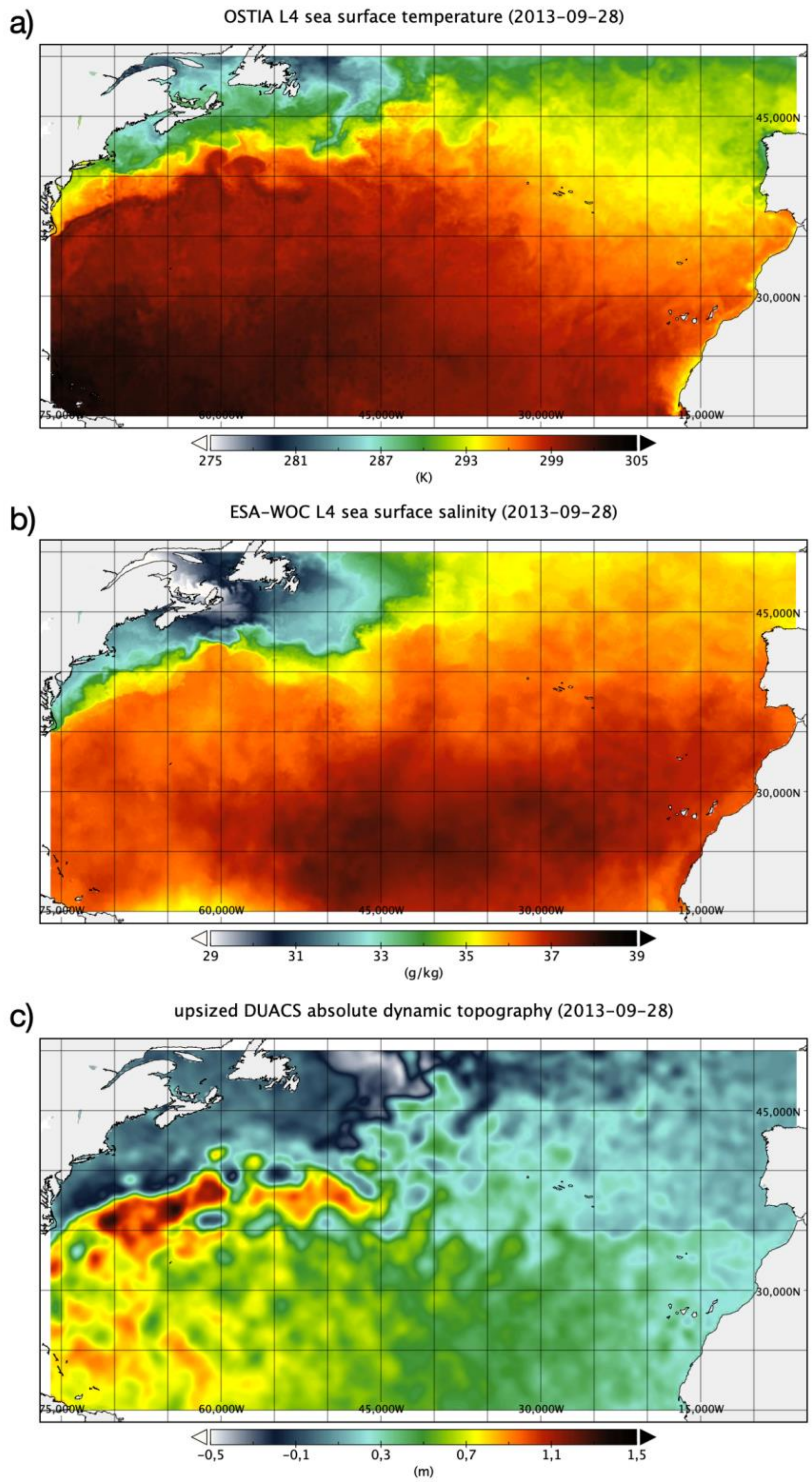

Figure 1. Examples of the surface daily data taken as input to the reconstruction techniques: OSTIA L4 reprocessed SST (a), SSS L4 developed within ESA-WOC project (b), adjusted ADT L4 derived from DUACS data (c).

3 Reconstruction techniques

3.1 Multivariate Empirical Orthogonal Function reconstruction (mEOF-r)

The multivariate Empirical Orthogonal Function reconstruction (mEOF-r) was taken as reference for the retrieval of the 3D hydrographic fields. This methodology has been applied in many previous studies (Buongiorno Nardelli, 2013; Buongiorno Nardelli et al., 2006, 2012, 2017; Buongiorno Nardelli and Santoleri, 2005), and it is thus only briefly recalled hereafter. It starts by building a state vector by concatenating (normalized) temperature, salinity and steric heights anomaly profiles, and decomposing its variability in EOF modes (thus called multivariate EOF). Anomalies are defined with respect to monthly WOA13 data (linearly interpolated in time between the central day of each month, and through a cubic spline horizontally). The EOFs are computed from available in situ observations, and the decomposition is truncated to a maximum of three modes. The three elements in the state vector reconstructed from the truncated EOF that correspond to the surface are equated to the anomalies of SST, SSS and adjusted ADT. In this way, a linear system is obtained, the unknowns being the three EOF amplitudes. Once solved through a trivial matrix inversion, full profiles associated with each mode can be estimated and finally summed up to get the synthetic vertical reconstruction.

In order to account for local differences in the dynamics, the configuration proposed in Buongiorno Nardelli et al., (2017) has been adopted also here. The North Atlantic domain is divided into subdomains with a maximum extension of 30° both in latitude and in longitude. Multivariate EOFs are estimated considering only the in situ profiles collected within ±20 days with respect to the reconstruction day. To remove eventual discontinuities in the reconstruction, all neighbouring subdomains are overlapped by one half of their latitudinal and longitudinal extensions. In the grid points where multiple reconstructions are available, these are averaged out by bilinearly weighting them with the inverse of the distance to each subdomain centre. In some cases, two modes (or even one mode) may be sufficient to retrieve most of the variability and the reconstruction error may increase if more modes are added (more than 95% of the variance is generally explained by the selected modes). Consequently, the optimal number of modes for the 3D reconstruction is chosen by evaluating the mean hindcast error within each subdomain, so as to minimize the root mean square difference between the input profiles and the synthetic profiles reconstructed from corresponding in situ surface measurements.

3.2 Feed-forward neural networks

Feed-forward networks represent the simplest type of artificial neural networks and consist of one input layer (the input vector) and one output layer (the output vector) connected through a variable number of hidden layers (if that number is >1 we speak about a “deep network”). Each of the layers is made up by a variable number of units: the elements of the vectors in the case of the input/output layers, and the artificial “neurons” (or computing nodes) in the hidden layers. Each of the units in one layer is connected to all units in the following layer through weights that are estimated during the network training, and each computing node processes the sum of its weighted input by passing it through an activation function which provides the neuron’s output. FFNN networks are designed to model complex flows of information from the input to the output and are common candidates to solve non-linear regression problems. The definition of a proper model for each specific problem, however, requires optimizing the choice of several “hyper-parameters”, starting from the number of hidden layers, the number of units within each hidden layer, to the activation function to apply within each hidden layer. For a given architecture, network training also implies a number of additional choices. In fact, training is performed by minimising some model loss function while iteratively feeding the network with several input-output samples. Various algorithms exist to this aim, and the same network trained in a different way on the same data may indeed lead to different results ("local" optima). Different results can be obtained depending also on the number of iterations (epochs) considered.

Large feed-forward networks (in terms of number of layers/units) are prone to over-fitting, as distinct sets of neighbouring neurons might adjust to reproduce individual samples, leading to complex co-adaptations which would not allow to generalize the network to unseen data. Again, different strategies can be followed to avoid co-adaptation: the dropout approach followed here is described in section 3.4.

In our tests, two different input/output vectors have been initially considered. In the first case, somehow imitating simple multilinear regression approaches, the input vector was made up of: the target depth for the retrieval, the anomalies of SST, SSS and adjusted ADT (same as in mEOF-r), the latitude, longitude, and the day of the year projected on a circle (as in Sammartino et al., 2018), while the output included the co-located values of temperature, salinity and steric heights anomalies at the target depth. In the second configuration, the depth has been dropped from the input data and the concatenated temperature, salinity and steric heights anomaly profiles were taken as output (same as mEOF-r state vector). All vectors are preliminary normalized through min-max algorithm.

Several preliminary hyper-parameter tuning tests have been carried out, considering one to three hidden layers, and a variable number of units within each, ranging between 5 and 50, with a 5 units increase step. The sigmoid performed better than hyperbolic tangent as activation function. “*Adam*” was selected as network optimizer, taking the mean squared error as loss metrics. 15% of input samples were randomly kept as a holdout validation dataset at each iteration. The number of optimal training epochs was found by monitoring model performance (*early stopping*).

The performance of the first set of models (those retrieving values at individual depths) never improved with respect to the climatology, while a visible improvement was found in the second configuration, especially when the choosing two hidden layers. The successive tests were thus restricted to this latter configuration, significantly increasing the number of hidden units (tests were run with up to 5000 units per layer). The final FFNN architecture considered in the following, which further improved the reconstruction accuracy) includes 1000 units in the two hidden layers (above that number, performance substantially stabilized).

3.3 Long Short-Term Memory networks

Recurrent neural networks (RNN) can be described as sequences of sub-networks (also called “cells”) designed to include information from the previous cell in a sequence as input to the successive one. This makes them particularly fit to model ordered sequences of data. Simple recurrent networks, however, are not able to efficiently process information from cells that lie too far along the sequence, due to vanishing/exploding values in the gradient-descent based optimizations.

Long Short-Time Memory (LSTM) network is a particular type of RNN, that is specifically designed to avoid vanishing/exploding gradients and preserve the relevant information flow throughout the network (Hochreiter and Schmidhuber, 1997). Within LSTM cells, the external input vector (x_i) is concatenated to the previous cell hidden state (h_{i-1}) and then passed through different "gates", each one aimed at carrying out a specific task to update both the hidden state itself (h_i) and a cell state (C_i), that is directly transmitted to the next cell and basically acts as a network "memory". The LSTM cell specifically includes a forget gate, an input gate, and an output gate, as depicted in figure 2a:

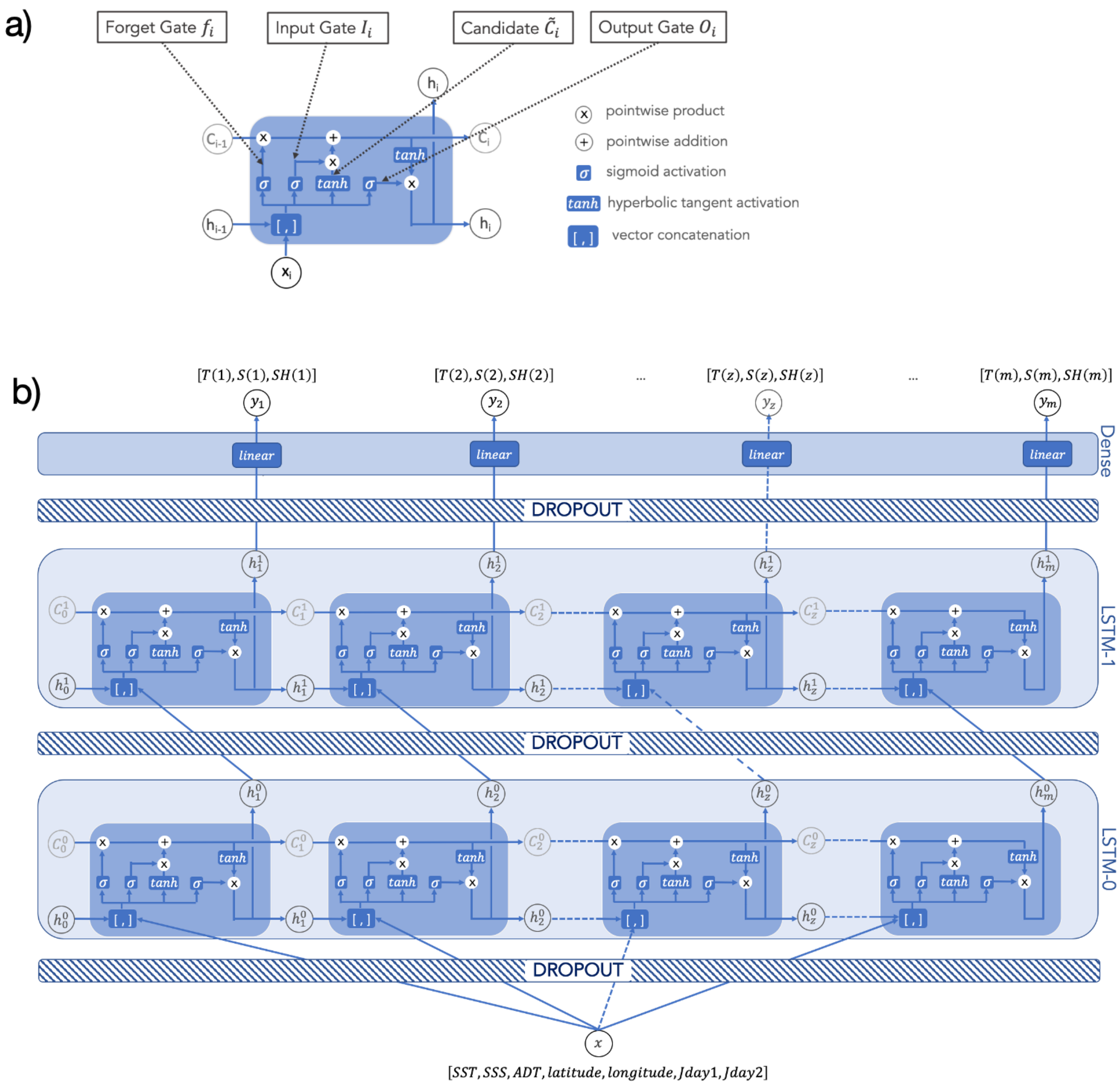

Figure 2. Diagram showing the elements of a single LSTM cell (a). Stacked LSTM model for the reconstruction of vertical hydrographic profiles (b).

whose equations thus read:

$$f_i = \sigma\left(W_f[h_{i-1}, x_i] + b_f\right)$$

$$I_i = \sigma(W_I[h_{i-1}, x_i] + b_I)$$
$$\tilde{C}_i = tanh(W_C[h_{i-1}, x_i] + b_C)$$
$$O_i = \sigma(W_O[h_{i-1}, x_i] + b_O)$$
$$C_i = f_i * C_{i-1} + I_i * \tilde{C}_i$$
$$h_i = O_i * tanh(C_i)$$

where σ and $tanh$ represent the sigmoid and hyperbolic tangent activation functions, respectively.

LSTM networks can include a single layer of LSTM cells or multiple LSTM layers stacked one on top of the other, potentially leading to quite deep architectures. The number of cells in each layer matches the length of the sequence by definition, but the number of hidden units still needs to be configured.

Here, the sequential information to exploit is provided by a multivariate output state vector comprising temperature, salinity and steric height anomaly profiles. In practice, each cell in the sequence considers in input the same surface values (i.e. the anomalies of SST, SSS and adjusted ADT), but takes as the output values at increasing depths (with depth “acting” as time in more standard applications of LSTM). As for FFNN models, all vectors are scaled within the 0-1 range before feeding the network.

The number of hidden units considered ranged between 5 and 50, with a 5 units increase step, and three different network architectures have been tested: a simple LSTM and two stacked LSTMs (with 2 and 3 layers each). The optimization algorithm and related parameters were exactly the same used for the FFNN reconstruction training, as well as the dropout strategy applied to avoid overfitting and obtain reconstructed profile uncertainties (see next section).

The best performance was obtained with a 2-layers stacked network, including 35 hidden units in each LSTM layer, as depicted in figure 2b.

3.4 Monte-Carlo Dropout

Standard dropout consists in randomly excluding a percentage of units during network training. Dropout provides a very efficient regularization strategy if applied during training, significantly reducing the risk of co-adaptation, thus limiting overfitting and improving model performance (Hinton et al., 2012; Srivastava et al., 2014). Moreover, dropout provides also an extremely simple and powerful approach to quantify a neural network uncertainty, if applied during both training and testing. In fact, running a regression neural network several times with dropout during testing generates different output for the same input. It was shown mathematically that these output are equivalent to Monte-Carlo sampling (Gal and Ghahramani, 2016). Hence, ensemble mean and variance provide the network’s output values and related uncertainty, respectively. During learning, 20% of the units have been dropped here.

4 Technique assessment

The assessment of the techniques has been performed by estimating temperature and salinity root mean squared differences (RMSD) with respect to fully independent test data (fig.3). To this aim, a randomly selected 15% of the 35344 in situ profiles collected in the area (totalling 5125 profiles) have been excluded from the network training. All techniques considered process anomalies with respect to WOA13 data, and are thus intended as corrections to the climatological profiles. Climatological temperature RMSD attains around 1.5°C at the surface, reaches a maximum of up to 1.7°C at ~100 m depth (at the base of the upper mixed layer) and then gradually decreases to the minimum error <0.25 °C at 1500 m, with a wide secondary maximum positioned around 500 m characterized by errors >1°C down to 800 m. The temperature retrieved with mEOF-r shows a moderate improvement in the upper 100 m and then in the 200-900 m layer, but then significantly degrades the climatology below 900 m. Conversely, both the FFNN with 2 hidden layers (each with 1000 units) and the stacked LSTM (with 2 layers and 35 hidden units in each cell) significantly improve the reconstruction all along the water column. Noticeably, LSTM clearly outperforms any of the other methodologies, with a RMSD never exceeding 1°C, and attaining below 0.75°C already at 200 m depth. Salinity RMSD show similar behaviours, with the climatological estimates reaching up to ~0.5 g/kg, and remaining above 0.2 in the upper 600 m, the mEOF-r displaying only a partial improvement in the upper 100 m (keeping its error close to that associated with the surface input data, i.e. around 0.25 g/kg), and FFNN and LSTM reducing the RMSD to almost one half, the LSTM further improving in the 200-800 m layer (fig. 3b).

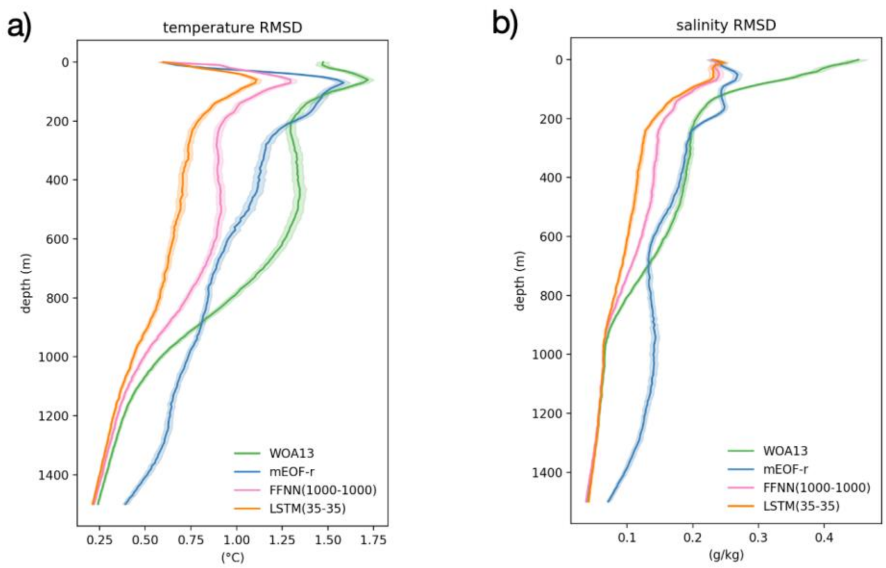

Figure 3. RMSD between temperature (a) and salinity (b) climatological and reconstructed profiles. RMSD confidence intervals (one σ) have been estimated with bootstrapping, and they are displayed here as shadowed areas.

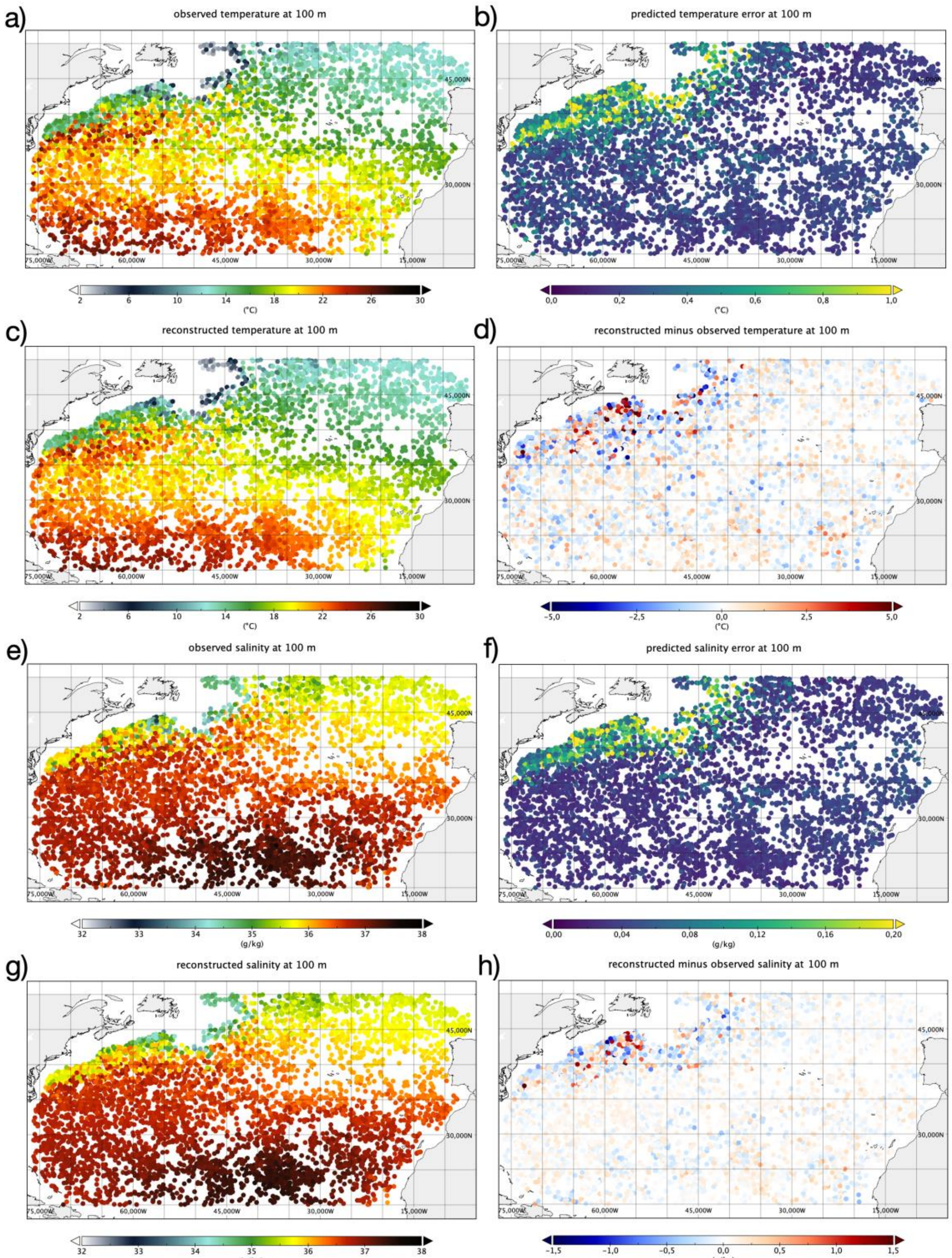

Figure 4. Independent observations of temperature (a) and salinity (e) at 100 m depth and corresponding LSTM reconstructions (c, g); temperature (b) and salinity (f) predicted LSTM reconstruction error and temperature (d) and salinity (h) differences between test data and synthetic reconstructions at 100 m.

As anticipated, the neural network methods coupled with Monte-Carlo dropout present another significant advantage with respect to mEOF-r and similar statistical reconstruction techniques, being able to deliver not only retrieved values, but also associated uncertainties. Comparing RMSD predicted by the LSTM with observed differences between test data and synthetic reconstructions at 100 m shows consistent patterns (clearly related to the areas where mesoscale variability is strongest, i.e. the Gulf Stream), both in the temperature and salinity fields (fig.4).

5 Conclusions

We have developed an innovative deep learning algorithm to project sea surface satellite observations at depth after learning from sparse co-located in situ hydrographic data. The proposed technique, based on a stacked Long Short-Term Memory neural network, coupled to a Monte-Carlo dropout approach, provides vertical profiles and associated uncertainties, outperforming both neural network reconstructions based on simpler feed-forward networks and multivariate EOF reconstruction. This technique will find immediate application for the development of a 3D product covering the North Atlantic in the framework of the European Space Agency World Ocean Circulation project (ESA-WOC). The work described here, however, covers only the development and assessment of the LSTM reconstruction methodology based on presently available data, as a new training of the network will be needed once updated ADT estimates will be made available by the project.

Remarkably, adaptation of this technique to other areas/periods is easy and straightforward. Simultaneous availability of uncertainties associated with individual profiles also suggests that this deep learning methodology could be tested to extend present data assimilation approaches in numerical models by ingesting consistent remotely sensed sea surface data and synthetic profile estimates.

Acknowledgments, Samples, and Data

I thank Daniele Ciani for providing upsized ADT data remapped over the study area, and Michela Sammartino and Francesca Elisa Leonelli for helpful discussions at the initial stage of the study.

The data used for the technique assessment can be found at https://doi.org/10.5281/zenodo.3943700.

References

Ballabrera-Poy, J., Mourre, B., Garcia-Ladona, E., Turiel, A. and Font, J.: Linear and non-linear T-S models for the eastern North Atlantic from Argo data: Role of surface salinity observations, Deep. Res. Part I Oceanogr. Res. Pap., 56(10), 1605–1614, doi:10.1016/j.dsr.2009.05.017, 2009.

Bao, S., Zhang, R., Wang, H., Yan, H., Yu, Y. and Chen, J.: Salinity profile estimation in the Pacific Ocean from satellite surface salinity observations, J. Atmos. Ocean. Technol., 36(1), 53–68, doi:10.1175/JTECH-D-17-0226.1, 2019.

Bittig, H. C., Steinhoff, T., Claustre, H., Fiedler, B., Williams, N. L., Sauzède, R., Körtzinger, A. and Gattuso, J. P.: An alternative to static climatologies: Robust estimation of open ocean CO2 variables and nutrient concentrations from T, S, and O2 data using Bayesian neural networks, Front. Mar. Sci., 5(SEP), 1–29, doi:10.3389/fmars.2018.00328, 2018.

Buongiorno Nardelli, B.: A Novel Approach for the High-Resolution Interpolation of In Situ Sea Surface Salinity, J. Atmos. Ocean. Technol., 29(6), 867–879, doi:10.1175/JTECH-D-11-00099.1, 2012.

Buongiorno Nardelli, B.: Vortex waves and vertical motion in a mesoscale cyclonic eddy, J. Geophys. Res. Ocean., 118(10), 5609–5624, doi:10.1002/jgrc.20345, 2013.

Buongiorno Nardelli, B.: A multi-year timeseries of observation-based 3D horizontal and vertical quasi-geostrophic global ocean currents, , (April), doi:10.5194/essd-2020-73, 2020.

Buongiorno Nardelli, B. and Santoleri, R.: Methods for the Reconstruction of Vertical Profiles from Surface Data: Multivariate Analyses, Residual GEM, and Variable Temporal Signals in the North Pacific Ocean, J. Atmos. Ocean. Technol., 22(11), 1762–1781, doi:10.1175/JTECH1792.1, 2005.

Buongiorno Nardelli, B., Cavalieri, O., Rio, M.-H. and Santoleri, R.: Subsurface geostrophic velocities inference from altimeter data: Application to the Sicily Channel (Mediterranean Sea), J. Geophys. Res., 111(C4), C04007, doi:10.1029/2005JC003191, 2006.

Buongiorno Nardelli, B., Guinehut, S., Pascual, a., Drillet, Y., Ruiz, S. and Mulet, S.: Towards high resolution mapping of 3-D mesoscale dynamics from observations, Ocean Sci., 8(5), 885–901, doi:10.5194/os-8-885-2012, 2012.

Buongiorno Nardelli, B., Guinehut, S., Verbrugge, N., Cotroneo, Y., Zambianchi, E. and Iudicone, D.: Southern Ocean Mixed-Layer Seasonal and Interannual Variations From Combined Satellite and In Situ Data, J. Geophys. Res. Ocean., doi:10.1002/2017JC013314, 2017.

Buongiorno Nardelli, B., Mulet, S. and Iudicone, D.: Three dimensional ageostrophic motion and water mass subduction in the Southern Ocean, J. Geophys. Res. Ocean., 2018.

Carrassi, A., Bocquet, M., Bertino, L. and Evensen, G.: Data assimilation in the geosciences: An overview of methods, issues, and perspectives, Wiley Interdiscip. Rev. Clim. Chang., 9(5), 1–50, doi:10.1002/wcc.535, 2018.

CATDS (2017). CATDS-PDC L3OS 2Q - Debiased daily valid ocean salinity values product from SMOS satellite. CATDS (CNES, IFREMER, LOCEAN, ACRI). doi:10.12770/12dba510-cd71-4d4f-9fc1-9cc027d128b0.

Ciani, D., Rio, M., Nardelli, B. B. and Etienne, H.: Improving the altimeter-derived surface currents using Sea Surface Temperature (SST) data : a sensitivity study to SST products, Remote Sens., 1–16, doi:10.3390/rs12101601, 2020.

Droghei, R., Buongiorno Nardelli, B. and Santoleri, R.: Combining in-situ and satellite observations to retrieve salinity and density at the ocean surface, J. Atmos. Ocean. Technol., 33, 1211–1223, doi:10.1175/JTECH-D-15-0194.1, 2016.

Droghei, R., Buongiorno Nardelli, B. and Santoleri, R.: A New Global Sea Surface Salinity and Density Dataset From Multivariate Observations (1993–2016), Front. Mar. Sci., 5(March), 1–13, doi:10.3389/fmars.2018.00084, 2018.

Forget, G., Campin, J. M., Heimbach, P., Hill, C. N., Ponte, R. M. and Wunsch, C.: ECCO version 4: An integrated framework for non-linear inverse modeling and global ocean state estimation, Geosci. Model Dev., 8(10), 3071–3104, doi:10.5194/gmd-8-3071-2015, 2015.

Fresnay, S., Ponte, A. L., Le Gentil, S. and Le Sommer, J.: Reconstruction of the 3-D Dynamics From Surface Variables in a High-Resolution Simulation of North Atlantic, J. Geophys. Res. Ocean., 123(3), 1612–1630, doi:10.1002/2017JC013400, 2018.

Gal, Y. and Ghahramani, Z.: Dropout as a Bayesian Approximation: Representing Model Uncertainty in Deep Learning, Proc. 33rd Int. Conf. Mach. Learn. New York, NY, USA, 48, 1050–1059 [online] Available from: http://ieeexplore.ieee.org/document/7350145/, 2016.

Gueye, M. B., Niang, A., Arnault, S., Thiria, S. and Crépon, M.: Neural approach to inverting complex system: Application to ocean salinity profile estimation from surface parameters, Comput. Geosci., 72, 201–209, doi:10.1016/j.cageo.2014.07.012, 2014.

Guinehut, S., Le Traon, P. Y., Larnicol, G. and Philipps, S.: Combining Argo and remote-sensing data to estimate the ocean three-dimensional temperature fields—a first approach based on simulated observations, J. Mar. Syst., 46(1–4), 85–98, doi:10.1016/j.jmarsys.2003.11.022, 2004.

Guinehut, S., Dhomps, a.-L., Larnicol, G. and Le Traon, P.-Y.: High resolution 3-D temperature and salinity fields derived from in situ and satellite observations, Ocean Sci., 8(5), 845–857, doi:10.5194/os-8-845-2012, 2012.

Hinton, G. E., Srivastava, N., Krizhevsky, A., Sutskever, I. and Salakhutdinov, R. R.: Improving neural networks by preventing co-adaptation of feature detectors, , 1–18 [online] Available from: http://arxiv.org/abs/1207.0580, 2012.

Hochreiter, S. and Schmidhuber, J.: Long Short-Term Memory, Neural Comput., 9(8), 1735–1780, doi:10.1162/neco.1997.9.8.1735, 1997.

Hutchinson, K., Swart, S., Meijers, A., Ansorge, I. and Speich, S.: Decadal-scale thermohaline variability in the Atlantic sector of the Southern Ocean, J. Geophys. Res. Ocean., 121(5), 3171–3189, doi:10.1002/2015JC011491, 2016.

Isern-Fontanet, J. and Hascoët, E.: Diagnosis of high-resolution upper ocean dynamics from noisy sea surface temperatures, J. Geophys. Res. Ocean., 119(1), 121–132, doi:10.1002/2013JC009176, 2014.

LaCasce, J. H. and Wang, J.: Estimating Subsurface Velocities from Surface Fields with Idealized Stratification, J. Phys. Oceanogr., (2), 150722131144001, doi:10.1175/JPO-D-14-0206.1, 2015.

Lapeyre, G.: Surface Quasi-Geostrophy, Fluids, 2(1), doi:10.3390/fluids2010007, 2017.

Liu, L. E. I., Xue, H. and Sasaki, H.: Reconstructing the ocean interior from high-resolution sea surface information, J. Phys. Oceanogr., 49(10), 3245–3262, doi:10.1175/JPO-D-19-0118.1, 2019.

Locarnini, R. A., Mishonov, A. V., Antonov, J. I., Boyer, T. P., Garcia, H. E., Baranova, O. K., Zweng, M. M., Paver, C. R., Reagan, J. R., Johnson, D. R., Hamilton, M. and Seidov, D.: World Ocean Atlas 2013. Vol. 1: Temperature., S. Levitus, Ed.; A. Mishonov, Tech. Ed.; NOAA Atlas NESDIS, 73(September), 40, doi:10.1182/blood-2011-06-357442, 2013.

Lu, W., Su, H., Yang, X. and Yan, X. H.: Subsurface temperature estimation from remote sensing data using a clustering-neural network method, Remote Sens. Environ., 229(April), 213–222, doi:10.1016/j.rse.2019.04.009, 2019.

McWilliams, J. C.: A survey of submesoscale currents, Geosci. Lett., 6(1), doi:10.1186/s40562-019-0133-3, 2019.

Meijers, A. J. S., Bindoff, N. L. and Rintoul, S. R.: Estimating the four-dimensional structure of the southern ocean using satellite altimetry, J. Atmos. Ocean. Technol., 28(4), 548–568, doi:10.1175/2010JTECHO790.1, 2011.

Meinen, C. and Watts, D.: Vertical structure and transport on a transect across the North Atlantic Current near 42°N: Time series and mean, J. Geophys. Res. …, 105 [online] Available from: http://onlinelibrary.wiley.com/doi/10.1029/2000JC900097/full (Accessed 24 August 2013), 2000.

Moore, A. M., Martin, M. J., Akella, S., Arango, H. G., Balmaseda, M., Bertino, L., Ciavatta, S., Cornuelle, B., Cummings, J., Frolov, S., Lermusiaux, P., Oddo, P., Oke, P. R., Storto, A., Teruzzi, A., Vidard, A. and Weaver, A. T.: Synthesis of Ocean Observations Using Data Assimilation for Operational, Real-Time and Reanalysis Systems: A More Complete Picture of the State of the Ocean, Front. Mar. Sci., 6(March), 1–6, doi:10.3389/fmars.2019.00090, 2019.

Mulet, S., Rio, M.-H., Mignot, a., Guinehut, S. and Morrow, R.: A new estimate of the global 3D geostrophic ocean circulation based on satellite data and in-situ measurements, Deep Sea Res. Part II Top. Stud. Oceanogr., 77–80, 70–81, doi:10.1016/j.dsr2.2012.04.012, 2012.

Pilo, G. S., Oke, P. R., Coleman, R., Rykova, T. and Ridgway, K.: Patterns of Vertical Velocity Induced by Eddy Distortion in an Ocean Model, J. Geophys. Res. Ocean., 123(3), 2274–2292, doi:10.1002/2017JC013298, 2018.

Rio, M.-H., Santoleri, R. and Bourdalle-Badie, R.: Improving the Altimeter-Derived Surface Currents Using High-Resolution Sea Surface Temperature Data : A Feasability Study Based on Model Outputs, , 2769–2784, doi:10.1175/JTECH-D-16-0017.1, 2016.

Rio, M., Mulet, S. and Picot, N.: Beyond GOCE for the ocean circulation estimate: Synergetic use of altimetry, gravimetry, and in situ data provides new insight into geostrophic and Ekman currents, Geophys. Res. Lett., 41, 8918–8925, doi:10.1002/2014GL061773.Received, 2014.

Roberts-Jones, J., Fiedler, E. K. and Martin, M. J.: Daily, Global, High-Resolution SST and Sea Ice Reanalysis for 1985–2007 Using the OSTIA System, J. Clim., 25(18), 6215–6232, doi:10.1175/JCLI-D-11-00648.1, 2012.

Sammartino, M., Marullo, S., Santoleri, R. and Scardi, M.: Modelling the Vertical Distribution of Phytoplankton Biomass in the Mediterranean Sea from Satellite Data: A Neural Network Approach, Remote Sens., 10(10), 1666, doi:10.3390/rs10101666, 2018.

Sauzède, R., Bittig, H. C., Claustre, H., de Fommervault, O. P., Gattuso, J. P., Legendre, L. and Johnson, K. S.: Estimates of water-column nutrient concentrations and carbonate system parameters in the global ocean: A novel approach based on neural networks, Front. Mar. Sci., 4(MAY), 1–17, doi:10.3389/fmars.2017.00128, 2017.

Srivastava, N., Hinton, G., Krizhevsky, A., Sutskeverm, I. and Salakhutdinov, R.: Dropout: A Simple Way to Prevent Neural Networks from Overfitting, J. Mach. Learn. Res., 15, 1929–1958, 2014.

Stammer, D., Balmaseda, M., Heimbach, P., Köhl, A. and Weaver, A.: Ocean Data Assimilation in Support of Climate Applications: Status and Perspectives, Ann. Rev. Mar. Sci., 8(1), annurev-marine-122414-034113, doi:10.1146/annurev-marine-122414-034113, 2016.

Stukel, M. R., Aluwihare, L. I., Barbeau, K. A., Chekalyuk, A. M., Goericke, R., Miller, A. J., Ohman, M. D., Ruacho, A., Song, H., Stephens, B. M. and Landry, M. R.: Mesoscale ocean fronts enhance carbon export due to gravitational sinking and subduction, Proc. Natl. Acad. Sci., 114(6), 1252–1257, doi:10.1073/pnas.1609435114, 2017.

Szekely, T., Gourrion, J., Pouliquen, S. and Reverdin, G.: The CORA 5.2 dataset for global in situ temperature and salinity measurements: Data description and validation, Ocean Sci., 15(6), 1601–1614, doi:10.5194/os-15-1601-2019, 2019.

Ubelmann, C., Cornuelle, B. D. and Fu, L.-L.: Dynamic Mapping of Along-Track Ocean Altimetry : Method and Performance from Observing System Simulation Experiments, , 33, 1691–1699, doi:10.1175/JTECH-D-15-0163.1, 2016.

Wang, J., Flierl, G., LaCasce, J. H., McClean, J. L. and Mahadevan, A.: Reconstructing the Ocean's Interior from Surface Data, J. Phys. … [online] Available from: http://journals.ametsoc.org/doi/abs/10.1175/JPO-D-12-0204.1 (Accessed 24 August 2013), 2013.

Wu, X., Yan, X. H., Jo, Y. H. and Liu, W. T.: Estimation of subsurface temperature anomaly in the North Atlantic using a self-organizing map neural network, J. Atmos. Ocean. Technol., 29(11), 1675–1688, doi:10.1175/JTECH-D-12-00013.1, 2012.

Yan, H., Wang, H., Zhang, R., Chen, J., Bao, S. and Wang, G.: A Dynamical-Statistical Approach to Retrieve the Ocean Interior Structure from Surface Data: SQG-mEOF-R, J. Geophys. Res. Ocean., (February), doi:10.1029/2019jc015840, 2020.

Zweng, M. M., Reagan, J. R., Antonov, J. I., Mishonov, A. V., Boyer, T. P., Garcia, H. E., Baranova, O. K., Johnson, D. R., Seidov, D. and Bidlle, M. M.: World Ocean Atlas 2013, Volume 2: Salinity, NOAA Atlas NESDIS, 119(1), 227–237, doi:10.1182/blood-2011-06-357442, 2013.